

See discussions, stats, and author profiles for this publication at: <https://www.researchgate.net/publication/266947020>

# Emergence of Chirality in Hexagonally Packed Mono layers of Hexapentyloxytriphenylene on Au(111): A Joint Experimental and Theoretical Study

ARTICLE *in* LANGMUIR · OCTOBER 2014

Impact Factor: 4.46 · DOI: 10.1021/la5030058 · Source: PubMed

---

READS

19

## 7 AUTHORS, INCLUDING:



Piotr Słeczkowski

Ewha Womans University

3 PUBLICATIONS 1 CITATION

[SEE PROFILE](#)



Nathalie Katsonis

University of Twente

46 PUBLICATIONS 1,813 CITATIONS

[SEE PROFILE](#)



Oleksiy Kapitanchuk

M.M.Bogolyubov Institute for Theoretical Phys...

24 PUBLICATIONS 72 CITATIONS

[SEE PROFILE](#)



Bernard Croset

Pierre and Marie Curie University - Paris 6

1 PUBLICATION 0 CITATIONS

[SEE PROFILE](#)

## Emergence of Chirality in Hexagonally Packed Monolayers of Hexapentyloxytriphenylene on Au(111): A Joint Experimental and Theoretical Study

Piotr Słeczkowski,<sup>†,‡,§</sup> Nathalie Katsonis,<sup>§</sup> Oleksiy Kapitanchuk,<sup>||</sup> Alexandre Marchenko,<sup>⊥</sup> Fabrice Mathevet,<sup>#</sup> Bernard Croset,<sup>\*,†,‡</sup> and Emmanuelle Lacaze<sup>\*,†,‡</sup>

<sup>†</sup>CNRS UMR7588, Institut des Nano-Sciences de Paris (INSP), 75252 Paris, France

<sup>‡</sup>UPMC Univ Paris 06, UMR 7588, Institut des Nano-Sciences de Paris (INSP) 75252 Paris, France

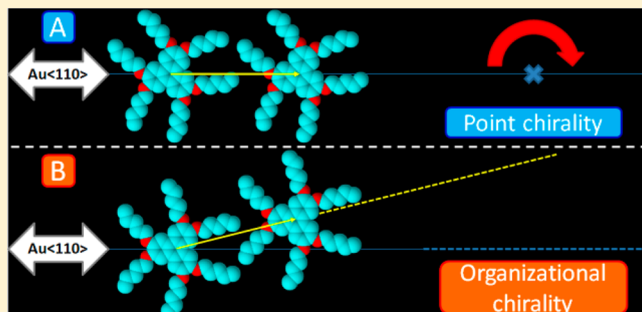
<sup>§</sup>Laboratory for Biomolecular Nanotechnology, MESA+ Institute for Nanotechnology, University of Twente, 7522 NB Enschede, The Netherlands

<sup>||</sup>Bogolyubov Institute for Theoretical Physics, National Academy of Sciences of Ukraine, Kiev-30 252601, Ukraine

<sup>⊥</sup>Institute of Physics, National Academy of Sciences of Ukraine, Kiev-30 252601, Ukraine

<sup>\*</sup>UPMC Univ Paris 06, UMR 8232, Institut Parisien de Chimie Moléculaire, Equipe Chimie des Polymères, 75005 Paris, France

**ABSTRACT:** We investigate the expression of chirality in a monolayer formed spontaneously by 2,3,6,7,10,11-pentyloxytriphenylene (HST) on Au(111). We resolve its interface morphology by combining scanning tunneling microscopy (STM) with theoretical calculations of intermolecular and interfacial interaction potentials. We observe two commensurate structures. While both of them belong to a hexagonal space group, analogical to the triangular symmetry of the molecule and the hexagonal symmetry of the substrate surface, they surprisingly reveal a 2D chiral character. The corresponding breaking of symmetry arises for two reasons. First it is due to the establishment of a large molecular density on the substrate, which leads to a rotation of the molecules with respect to the molecular network crystallographic axes to avoid steric repulsion between neighboring alkoxy chains. Second it is due to the molecule–substrate interactions, leading to commensurable large crystallographic cells associated with the large size of the molecule. As a consequence, molecular networks disoriented with respect to the high symmetry directions of the substrate are induced. The high simplicity of the intermolecular and molecule–substrate van der Waals interactions leading to these observations suggests a generic character for this kind of symmetry breaking. We demonstrate that, for similar molecular densities, only two kinds of molecular networks are stabilized by the molecule–substrate interactions. The most stable network favors the interfacial interactions between terminal alkoxy tails and Au(111). The metastable one favors a specific orientation of the triphenylene core with its symmetry axes collinear to the Au⟨110⟩. This specific orientation of the triphenylene cores with respect to Au(111) appears associated with an energy advantage larger by at least 0.26 eV with respect to the disoriented core.



### INTRODUCTION

It is well-known that a number of achiral molecules adsorbed on crystalline substrates can form 2D chiral structures.<sup>1,2</sup> This emergence of 2D chirality corresponds to a symmetry breaking induced by interactions with the substrate underlying the molecular monolayers. However, in the large majority of 2D systems reported to date, the chiral domains remain of limited extension, and mirror image domains are formed. Therefore, the surface–monolayer system remains racemic at the macroscopic scale. More recently, a number of studies evidenced the possibility to favor specific 2D monolayers chiral plane groups, either by using chiral solvents,<sup>3,4</sup> a sergeant-and-soldiers approach,<sup>5–7</sup> or chiral auxiliaries.<sup>8–11</sup> As a consequence, a precise understanding of how the interplay between molecule/

substrate and molecule/molecule interactions allows the emergence of extended chiral domains in 2D, becomes of primary importance. Many STM investigations concerning supramolecular chirality at the liquid/solid interface have focused either on the influence of the substrate<sup>1</sup> or on the influence of specific molecule/molecule interactions, for example hydrogen bonding<sup>12–17</sup> or covalent bonding.<sup>18</sup> Some antiferromagnetic-like coupling between molecules has also been demonstrated.<sup>19</sup> One system, however, displayed chirality

Received: July 28, 2014

Revised: September 30, 2014

Published: October 15, 2014



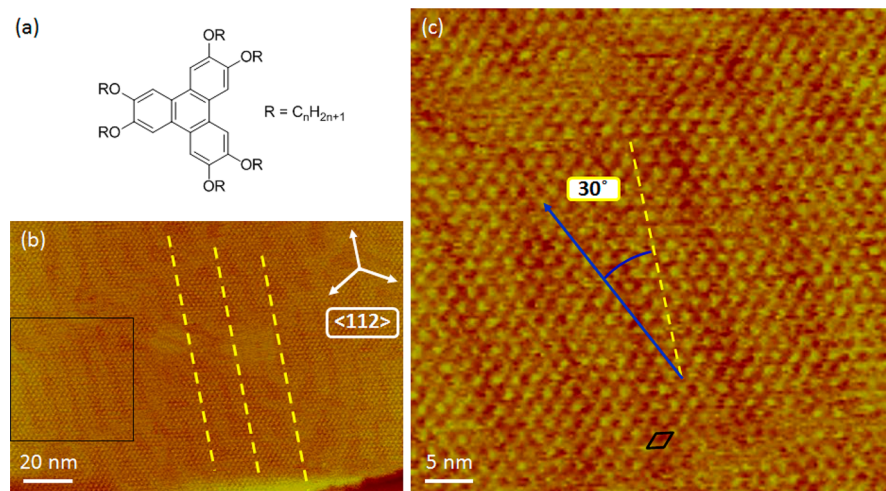


**Figure 1.** (a) Schematic representation of hexakis-2,3,6,7,10,11-alkoxytriphenylene, a molecule belonging to the  $D_{3h}$  point-symmetry group. (b,c) STM images of HST molecules self-assembled at the  $n$ -tetradecane/Au(111) interface. Yellow dashed-lines highlight the main direction of Au(111) reconstruction parallel to the  $\langle 112 \rangle$  crystallographic directions of the substrate. Black square in panel b represents the zoomed area shown in panel c. Black diamond in panel c represents the primitive unit cell of the HST monolayer physisorbed at Au(111);  $I_t = 5$  pA,  $V_t = 100$  mV.

for simple steric and van der Waals molecule–substrate and molecule–molecule interactions, HtB-HBC on Cu(110).<sup>20,21</sup>

Here, we confirm that the balance between steric and van der Waals molecule/substrate and intermolecular interactions can promote the formation of 2D chiral domains, thanks to the necessity for the molecular system to increase its density on the substrate. This is shown for 2,3,6,7,10,11-hexapentyloxytriphenylene (HST), a model (archetypal) molecule composed by an aromatic core that is symmetrically substituted by six alkoxy chains containing five carbons each. This achiral molecule presents a 3-fold symmetry, analogous to the 6-fold symmetry of the underlying gold surface. Upon self-assembly, a hexagonal network is formed, leading to an STM contrast without any sign of chirality.<sup>1</sup> However, using the observation of metastable domains by STM, together with calculations of steric van der Waals interactions between molecules, we establish the symmetry breaking associated with the presence of two kinds of domains: a stable and a metastable one. Analyzing the molecular orientations within the two domains, we demonstrate that the Au(111)/triphenylene core interaction is more favorable for a specific orientation of the core, is close to being parallel to the Au(110) direction, and is responsible for the appearance of the metastable domain. We estimate the corresponding energetic advantages and reveal the induced chirality of the two domains. The observation of density-driven symmetry breaking with simple symmetric molecules suggests that a large number of physisorbed molecules are likely to present a similar behavior.

## ■ EXPERIMENTAL SECTION

The Au(111) substrate was purchased from Neyco, and consisted of a 150 nm gold layer evaporated onto a mica support. Annealing with a gas flame (propane–air) was performed until signs of glowing appeared on the sample. 2,3,6,7,10,11-hexapentyloxytriphenylene (HST) has been synthesized and characterized within the Laboratoire de Chimie des Polymères, Université Pierre et Marie Curie (Paris, France). Additional purification by the column chromatography has been performed, and material from several batches has been used for further studies. HST is a discotic liquid crystal that exhibits a hexagonal columnar mesophase in bulk between 69 and 122 °C.<sup>22</sup> HST was dissolved in  $n$ -tetradecane (Sigma-Aldrich, pure >99%, used as received) with a concentration of 1.67 mmol/L. The solution was

heated up to ~70 °C for 15 min prior to deposition onto freshly flame-annealed gold. A 50 μL droplet of this solution was deposited onto the gold substrate. Two kinds of depositions were performed onto Au(111) substrates. One was onto hot substrate, at 100 °C, the second one was onto cold substrate, at ambient temperature. The STM tip was mechanically cut from a Pt/Ir wire (90/10 wt %, GoodFellow, Inc.) and was immersed in the droplet after cooling back, for the scanning process. The structures of monolayers were investigated using Bruker-multimode SA with low-current head. Typical imaging conditions in constant current mode were 100–500 mV for the tip voltage and 5–50 pA for the tunneling current. All STM imaging was carried out at room temperature.

## ■ RESULTS

Figure 1b,c represents typical STM images recorded following the deposition of an HST/ $n$ -tetradecane droplet on a heated ( $T = 100 \pm 1$  °C) Au/mica sample, just after flame-annealing the substrate.<sup>23</sup> Bright spots are clearly organized into hexagonal mesh. In accordance to the well-known fact of strong contribution of aromatic motifs to the STM contrast,<sup>24</sup> we infer that those bright spots resemble the central triphenylene cores. Moreover, it should be noticed that all molecular rows are aligned along the  $\langle 110 \rangle$  crystallographic direction of Au(111), since they form a 30° angle with the gold reconstruction, this latter one being featured by yellow dashed-lines in Figure 1. The fact that Au(111) reconstruction is not lifted as a result of the monolayer formation suggests that the discotic molecules are physisorbed. Lack of any periodic variation of STM contrast within the observed monolayers suggests that the physisorption has occurred at energetically equal adsorption sites. This situation was preserved throughout subsequent scans, for different scanning directions, tip-sample polarities and tunneling current parameters. The value of distance between two nearest neighbors, equal  $2.0 \pm 0.1$  nm, is obtained from the analysis of STM images. The molecular rows being oriented along  $\langle 110 \rangle$ , this value must be compared to the corresponding Au(111) period, equal to 0.288 nm. This leads to the conclusion that the distance between two neighboring HST molecules is equal to seven times the distance between two gold atoms along the  $\langle 110 \rangle$  crystallographic direction of Au(111). It is worth noting that the observed period value of 2 nm is very close to the bulk columnar period of the liquid

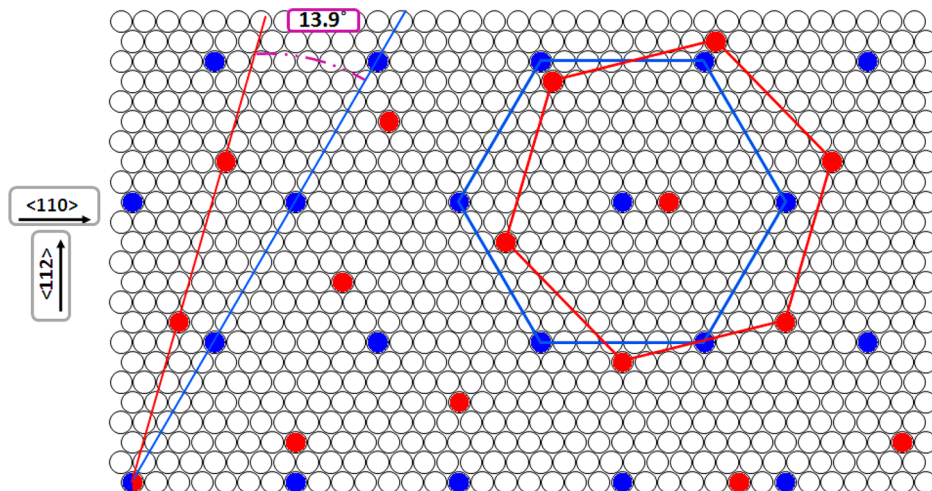


**Figure 2.** Proposed model of packing of HST at an *n*-tetradecane/Au(111) interface for  $(7 \times 7)$  and  $(\sqrt{52} \times \sqrt{52})R13.9^\circ$  domains, indicated by a blue- and a red-color mesh, respectively.

**Table 1. Comparison of 2D Model Lattices Illustrated in Figure 6**

mesh	lattice parameter $r$ [nm]	relative surface density <sup>a</sup>	mesh rotation angle vs Au<110>	intermolecular rotation minima $\phi_i^0$ [°]	triphenylene orientation <sup>b</sup> $\beta$ [°]	alkyl chain orientation vs Au<110>
M1	1.728	1.361	0.0			
M6	1.799	1.256	16.1			
M2	1.889	1.140	7.6			
M10	1.995	1.021	30.0	13.6	-16.4 16.4	-1.4 1.4 28.6 -28.6
M0	2.016	[-]	0.0	13.6	13.6 -13.6	-1.4 1.4 28.6 -28.6
M7	2.016	1.000	21.8	13.6	8.2 24.6	-6.8 9.6 23.2 -20.4
M3	2.077	0.942	13.9	13.5	0.4 27.4	-14.6 12.4 15.4 -17.6
M4	2.174	0.860	6.6			
M9	2.286	0.778	19.1			
M5	2.304	0.766	0.0			
M8	2.249	0.803	26.3			

<sup>a</sup>With their geometrical parameters related to the thermodynamically stable  $(7 \times 7)$  mesh (M0). <sup>b</sup>Final orientations of the central triphenylene cores are presented with respect to Au<110> crystallographic direction of substrate ( $\beta = 0^\circ$  stands for molecular symmetry axes (see Figure 4) pointing along Au<112>). For each mesh, its corresponding angular value of interaction energy minimum ( $\phi_i^0$ ) is also considered, except for the sterically forbidden (M1, M6, and M2) and low surface-density structures (M4, M8, M9, and M5). Alkyl chains orientations vs Au<110> are also indicated.

crystal phase,<sup>22</sup> and thus the 2D monolayer presents a compactness comparable to the bulk one. This latter characteristics appear in contrast with the HST 2D monolayers on graphite, which display a smaller period than the bulk one.<sup>19</sup>

The schematic representation of the packing of HST molecular nodes at the *n*-tetradecane/Au(111) interface is illustrated by the blue hexagonal mesh in Figure 2, and may be denoted by  $(7 \times 7)$  according to Woods terminology. We call it in the following M0 mesh (Table 1).

Surprisingly, when deposition of HST/*n*-tetradecane solution is performed on a cold substrate, i.e., not directly after its flame-annealing, STM images also reveal that another type of domain usually coexists with  $(7 \times 7)$  domains on Au(111), which may correspond to a metastable HST network. The situation is depicted by Figure 3, where  $(7 \times 7)$  domain areas (A), and the “cold-deposition” domain areas (B) are emphasized by blue and red lineaments, respectively. A detailed study of the lateral distances between triphenylene cores in A and B areas provides

a value of  $2.0 \pm 0.1$  nm for the periodicity of lattice nodes in both kinds of domains. As in the previous case, no sign of periodic variation of STM contrast of probed self-assemblies is observed, suggesting commensurability of both A and B domains. Drift-corrected image analysis resulted in determination of the angle between respective unit vectors of A and B unit cells:  $14 \pm 1^\circ$ . Taking into account all geometrical features of B-type domains obtained from STM measurements, one may construct a model that theoretically corresponds to the observed unit cell. The hexagonal mesh of the 2D crystal presented in Figure 2 with a red color corresponds to the second type of domain found after “cold-deposition”. Its theoretical nearest neighbor distance value equals 2.077 nm, with the unit cell vectors rotated by  $13.9^\circ$  from previously found  $(7 \times 7)$  domain. It may be denoted as  $(\sqrt{52} \times \sqrt{52})R13.9^\circ$  in Woods terminology (M3 mesh; Table 1). Comparison of panels a and b in Figure 3 obtained on the

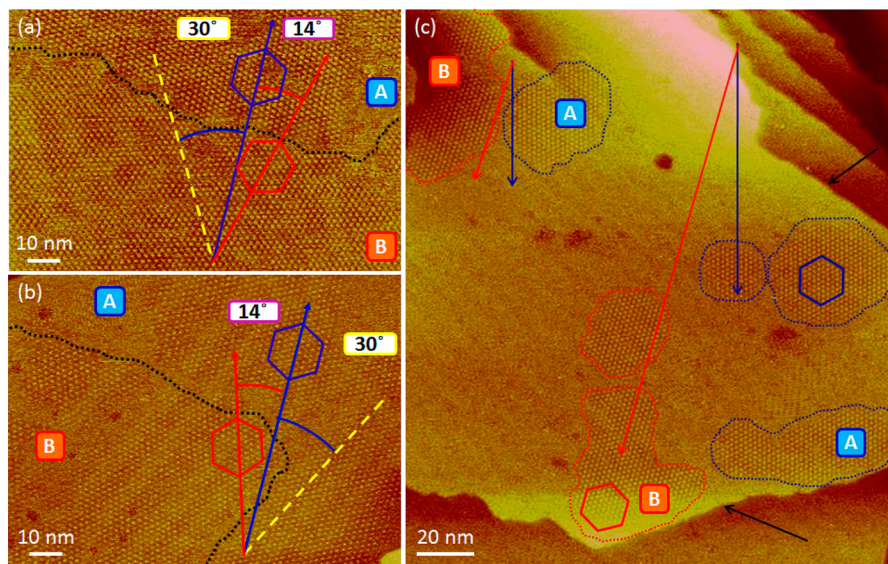


**Figure 3.** STM images of twofold orientation of HST molecules self-assembled at the *n*-tetradecane/Au(111) interface. (7 × 7) domains (A) and ( $\sqrt{52} \times \sqrt{52}$ )R13.9° domains (B) are depicted by blue and red graphics, respectively. Yellow dashed-lines in panels a and b highlight the main direction of Au(111) reconstruction, i.e., the ⟨112⟩ directions. Black dotted-lines in panels a and b highlight the domain boundaries. (a,b) STM pictures are taken on the same Au(111) monocrystal and evidence the two possible orientations of B domains, rotated by  $\pm 13.9^\circ$  from the A ones. Black arrows in panel c show the step-edges of Au(111) substrate, parallel to the A-domains dense directions, which confirm an orientation along ⟨110⟩ for the (7 × 7) mesh;  $I_t = 10$  pA,  $V_t = 100$  mV.

same sample evidence the two possible orientations of M3 domains, i.e.,  $13.9^\circ$  and  $-13.9^\circ$ .

Knowing that the 2D crystals formed by the HST mesogens are commensurate does not give clear view on the driving force behind the self-assembly process, since no information can be obtained concerning the mutual orientation of the molecules within the monolayer or with respect to the surface. It should be recalled that physisorbed self-assemblies find their origin in the subtle interplay between intermolecular and interfacial interactions. Due to the structural dichotomy of HST, one may expect competition between its two components: the triphenylene core and the pentyloxy chains, since they are likely to display different relative affinities to the substrate.<sup>25,26</sup> The obstacle in analysis of HST monolayers on Au(111) results from the fact that molecules are visualized as blurred spots, as soon as the scale that normally should enable intramolecular resolution is attained. In particular, alkoxy chains are never visible, in connection with their mobility, despite the fact that they may also present a well-defined average location on the substrate.

We have thus used theoretical calculations to provide further insight into the geometry of the system. We have started by considering a single molecule to estimate the orientation of alkoxy chains on average with respect to the central triphenylene core. Figure 4 represents the optimized geometry of an isolated HST molecule calculated by density functional theory (DFT/B3Lyp/6-31G\*). As may be noticed, HST retains its 3-fold symmetry, and the central triphenylene core, as expected for a polyconjugated moiety, remains flat. What should be further perceived is that each of the three equivalent sides of the triphenylene motif remains in the plane of the central part of the molecule, but is associated with two alkoxy chains bent apart by approximately  $15 \pm 1^\circ$ . This minimized energy conformation will serve us as a model molecular structure for the physisorbed monolayers.

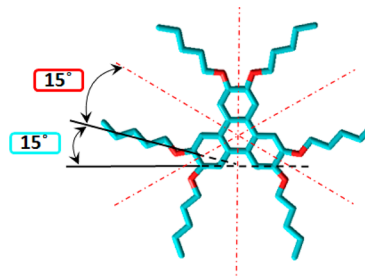


**Figure 4.** Optimized geometry of HST molecule calculated by density functional theory (DFT/B3Lyp/6-31G\*). Red dash-dotted lines that represent the symmetry axes of the molecule underline its affiliation to the  $D_{3h}$  symmetry group. The planar character of the molecule is very noticeable, with an important alkoxy chains deflection by  $15^\circ$  from the respective symmetry axis.

## DISCUSSION

In addition to the commensurability of the monolayer, for our investigations we have made two main assumptions. On one hand, molecules tend to maximize their packing density (together with alkyl chains lying flat on the surface) and thus minimize the adsorption energy of the system. On the other hand, we need to take into account the steric repulsion between each building block associated with the peripheral alkoxy parts.

We start with the intermolecular interaction,  $E_{\text{mol-mol}}$  and consider a pair of molecules uniformly oriented in one plane (as depicted on the top of Figure 5a) with a separation distance between centers of their masses,  $r$ , the lattice parameter. Possessing exact atomic coordinates, it is possible, by summing the Lennard-Jones (12-6 LJ) potential between each methylene group of the alkyl chains, to calculate the interaction between two molecules and probe the evolution of this interaction for unidirectional in-plane rotation of a molecular couple (Figure 5a). The Lennard-Jones potential between two methyl group is  $E_{\text{LJ}} = 4 \epsilon [(\sigma/d)^{12} - (\sigma/d)^6]$ ,  $\epsilon = 10.3$  meV and  $\sigma = 0.398$  nm

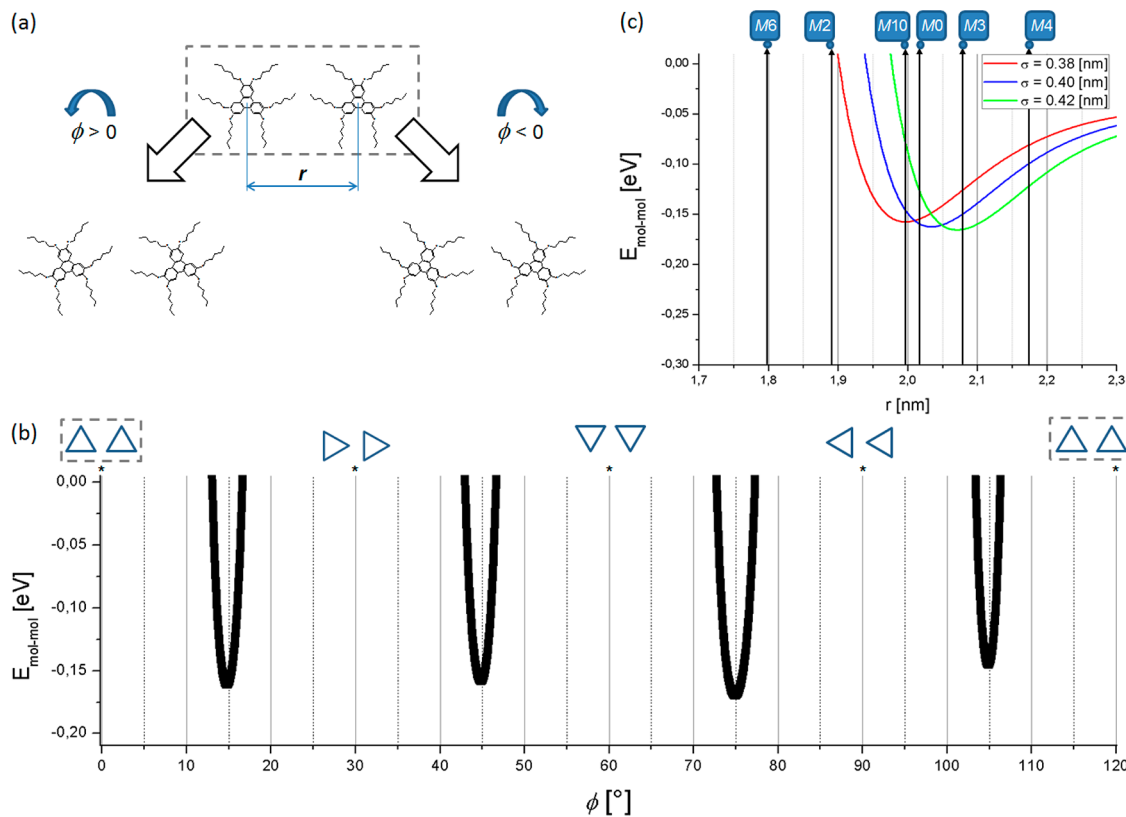


**Figure 5.** Two HST molecules with parallel directions and their schematic unidirectional in-plane rotation of angle  $\pm\phi$ .  $r$  stands for the distance between the centers of their masses (varying for different meshes, see Table 1). (b) Angular dependence of the Lennard-Jones intermolecular energy of interaction ( $E_{\text{mol-mol}}$ ) for the dimers shown in panel a with  $7 \times 7$  ( $M_0$ ) mesh parameter (i.e.,  $r = 2.016$  nm). Since HST belongs to the  $p6m$  symmetry group, energetically allowed regions appear periodically and exhibit a mirror symmetry about each  $(2k+1) \cdot 30^\circ$  value ( $k$  being an integer). Pairs of blue triangles symbolically show the orientation of the corresponding aromatic cores (angles marked with asterisks). (c) Lennard-Jones intermolecular interactions as a function of intermolecular distance,  $r$ , for different values of the  $\sigma$  parameter,  $\phi$  being optimized for each  $r$ . Lack of the non-negative part of the plot enables one to exclude  $M_6$  and  $M_2$  meshes (Table 1) from further considerations.

from ref 27. Angular dependence of this interaction is presented on Figure 5b for  $(7 \times 7)$  mesh. The energetically allowed range (i.e.,  $E < 0$ ) appears as a rather narrow angular region, which strictly defines the molecule orientation in the reference mesh. The interaction value, on the order of 0.15 eV, appears to be of the same order but smaller than the interaction between Au(111) and a  $\langle 110 \rangle$ -oriented  $C_5$ -carbon chain, equal to -0.53 eV,<sup>28</sup> suggesting that the attractive molecular interactions do not dominate the molecule/substrate interactions. Taking into account the value  $\phi_i^0 = 13.6^\circ$ , corresponding to the energy minimum, and the alkoxy chain deflection by  $15^\circ$  from the molecule's symmetry axis, we obtain that three out of six  $-C_5H_{11}$  chains of each HST molecule would be roughly oriented parallel to the Au $\langle 110 \rangle$ . It is well-known that  $\langle 110 \rangle$  is the preferred crystallographic direction for physisorption of alkanes on Au(111).<sup>29–32</sup> Alkyl chains may thus strongly contribute to the adsorption energy of  $(7 \times 7)$  domains. This result evidences the unexpected chirality of the  $(7 \times 7)$  mesh, associated with the rotation around  $\pm 13.6^\circ$  of the molecule with respect to the Au $\langle 110 \rangle$  direction. This is at the same time a point and an organizational chirality, the molecules being disoriented with respect to the 2D array as well. This chirality, in other words the  $13.6^\circ$  rotation of the molecule, could not be detected through the STM contrast only, due to the “invisibility” of the alkoxy chains. It appears to be of a very different nature with respect to the chirality demonstrated for the same molecules adsorbed on HOPG, the latter being

associated with different adsorption geometry of one molecule out of two.<sup>19</sup>

Alternative two-dimensional commensurate hexagonally packed meshes with near cell parameters must be considered. Altogether with the  $M_0$  mesh, we denote these structures  $M_1$ , ...  $M_{10}$ , according to numbered atomic sites shown in Figure 6. All of the characteristics of the constructed set of meshes, including the lattice parameter, are summarized in Table 1. The metastable  $(\sqrt{5}2 \times \sqrt{5}2)R13.9^\circ$  structure ( $M_3$ ) appears

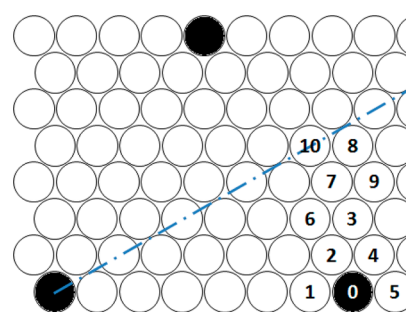


**Figure 6.** Schematic representation of the reference  $(7 \times 7)$  structure (black atomic sites,  $M_0$ ). Alternative meshes ( $M_1$ ...  $M_{10}$ ) are created on the basis of a unit vector of absolute value close to the one of the  $(7 \times 7)$  mesh. Each mesh is hooked at the center of the atom in the left-bottom corner and spans to the respective atomic site (numbered). Blue dash-dotted line points the mirror symmetry axis.

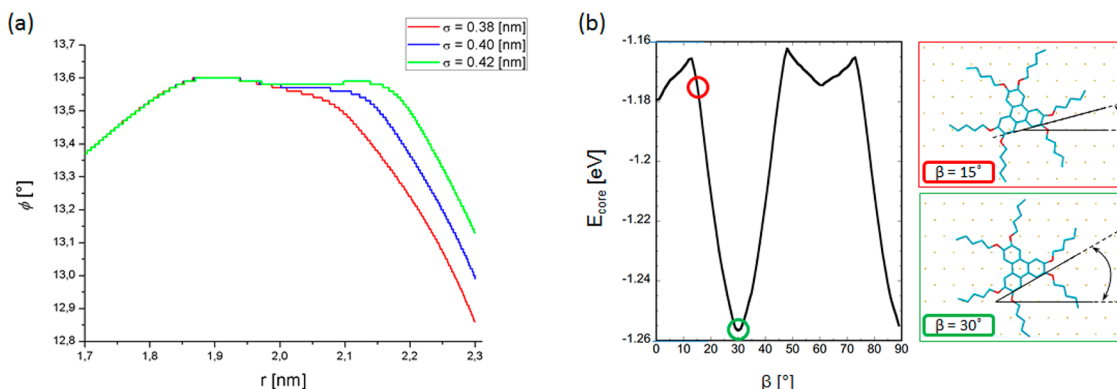


**Figure 7.** (a) The plot of  $\phi_i^0$  angle as a function of intermolecular distance, showing robustness with respect to  $\sigma$  variations. (b) Energy plot of molecule–substrate interactions based on a 12-6 LJ potential, as a function of the molecule rotation angle,  $\beta$  (Table 1). For this calculation, only the central triphenylene core has been taken into consideration (alkoxy tails excluded). Schemes in red and green boxes indicate the actual orientations of the core with respect to the substrate for the  $+15^\circ$  and  $+30^\circ$  rotations, respectively (the latter one being visibly favorable, since occupying the energetic minimum).

slightly less dense than  $M0$ . Computations of Lennard-Jones interactions are shown in Figure 5c, for molecule–molecule distances varying between 1.7 and 2.3 nm according to the variation of cell parameter from  $M0$  to  $M10$  (Table 1),  $\phi$  being optimized for each  $r$ . The phenomenological parameter  $\sigma$  was allowed to take three different values: 0.38, 0.40, and 0.42 nm. Figure 5c shows that steric considerations clearly exclude structures  $M1$  and  $M6$ , and that in order for the  $M2$  structure not to be excluded, the  $\sigma$  value must be equal to 0.38 nm, i.e., significantly lower than the standard value 0.398 nm. At this stage, we exclude  $M1$ ,  $M6$ , and  $M2$  structures for steric reasons and  $M4$ ,  $M8$ ,  $M9$ , and  $M5$  structures because their low surface densities lead to a remarkable loss in molecule–surface interactions. Figure 7a reveals an important result, the value of the angle  $\phi_i^0$  around  $14^\circ$  determined by steric consideration is common to all the structures, this result being robust with respect to  $\sigma$  variations. Like  $M0$ , the  $M10$ ,  $M3$ , and  $M7$  meshes exhibit molecule disorientation around  $14^\circ$  with respect to the crystallographic axis of the mesh. This finally leads to the same organizational chirality for all these structures. All of the  $\phi_i^0$  values for meshes considered in further investigations are indicated in Table 1, together with the triphenylene core orientation with respect to the substrate, represented by  $\beta$ .  $\beta = 0^\circ$  stands for molecular symmetry axes (see Figure 4) pointing along  $\text{Au}\langle 112 \rangle$ .

We must now understand the observation of  $M0$  and  $M3$  structures together with the nonobservation of  $M7$  and  $M10$  structures and thus evaluate the variations of molecule–substrate interactions. Table 1 shows that the orientations of the molecules with respect to the substrate are close for  $M0$  (which is observed) and  $M10$  (which is not observed) on one hand and for  $M3$  (which is observed) and  $M7$  (which is not observed) on the other hand. In the case of  $M0$  and  $M10$ , the molecule orientation allows three of the alkoxy chains to be parallel ( $M10$  case) or almost parallel ( $M0$  case, misfit angle of  $3^\circ$ ) to the  $\text{Au}\langle 110 \rangle$  direction, which is known to be an energetically favorable direction. In contrast, all the six alkoxy chains are misoriented for  $M3$  and  $M7$  structures.

In order to evaluate the interaction energy between the triphenylene core and the substrate,  $E_{\text{core}}$ , we have performed a summation of Lennard-Jones terms between the carbon atoms of the core and the Au atoms of the surface using  $\sigma_{\text{C–Au}} = 3.0 \text{ \AA}$  and  $\epsilon = 0.013 \text{ eV}$ .<sup>31</sup> The summation being done for all the

distances between interacting atoms inferior to  $2.5 \sigma_{\text{C–Au}}$ . Results are shown in Figure 7b:  $E_{\text{core}}$  is presented as a function of the core orientation with respect to the substrate,  $\beta$ , the position of the molecule being optimized for each value of this orientation. A strong minimum is observed for  $\beta = 30^\circ$ . This is consistent with the stabilization of the  $M3$  structure, which is observed despite the nonfavorable orientation of the alkyl chains, together with a lower density for  $M3$  with respect to  $M0$ . One of the initially allowed  $\beta$  value for  $M3$  of  $0.4^\circ$  may not be finally observed, as inferred from Figure 7b (Table 1). The other  $\beta$  value is not exactly  $30^\circ$ , but  $27.4^\circ$ . However, the  $2\text{--}3^\circ$  width of the potential well in Figure 5b (i.e.,  $4^\circ$ ) authorizes  $M3$  tilt from  $27.4^\circ$  to  $30^\circ$ . The value  $\beta = 24.6^\circ$  associated with  $M7$  may appear in contrast too far from the minimum of Figure 7b to allow for the stabilization of  $M7$  mesh in agreement with experimental nonobservations of  $M7$  by STM. On the other hand, no sensible energy differences in  $E_{\text{core}}$  are visible in Figure 7b between the orientations corresponding to  $M0$  and  $M10$ . The origin of the nonobservation of  $M10$  mesh is thus not clear. We may postulate that the core/Au potential may exhibit rapid variation with  $\beta$  not accounted by our model. This suggests that the flexibility of the molecule should be taken into account to refine the model. Accordingly, the numerical values of Figure 7b do not quantitatively describe the experimental data. The potential well at  $30^\circ$  is not deep enough to account for the stabilization of  $M3$  with a density lower by 6% with respect to  $M0$ . Taking into account the known energy of adsorption for the  $\langle 110 \rangle$ -oriented  $C_5$ -carbon chain, equal to  $-0.53 \text{ eV}$ ,<sup>28</sup> together with a  ${}^{M0}E_{\text{core}}$  value equal to  $-1.17 \text{ eV}$  (Figure 7b), we would expect  ${}^{M3}E_{\text{core}} - {}^{M0}E_{\text{core}}$  to be larger than  $0.26 \text{ eV}$ , i.e., 3 times more than the calculated potential well.

A major conclusion arising from the scenario depicted above is thus the dual origin of both H5T domains on  $\text{Au}(111)$ , driven by specific interaction of the substrate with either the polyaromatic core or the alkoxy chains and leading to a 2D chirality of both structures.  $M0$  is associated with organizational chirality, but  $M3$  is chiral as well, although corresponding to a different type of chirality. It is worth noticing that, generally speaking, for large molecules, if the molecule–substrate interactions are strong enough to impose commensurate structure, we expect emergence of point chirality structures. They correspond to meshes disoriented with respect to the dense crystallographic directions of the substrate, which must

exist if the intermolecular distance is significantly large with respect to the substrate period. This is the case of *M*10 and *M*3. However, the molecule–substrate interactions being strong enough to impose commensurability, usually it also leads to selection of specific chiral structure among all possible ones, here *M*3 only. For one given selected mesh, it also leads to selection of only a limited number of diastereoisomers among the possible ones, as already shown for HtB-HBC molecules on Cu(110).<sup>20,21</sup> For *M*3, combining point chirality together with the same chirality than *M*0, four diastereoisomers are expected.<sup>20,21</sup> We expect clockwise and counterclockwise orientations of the mesh, which are indeed observed as shown in Figure 3. Moreover, for each of these two meshes orientations, as shown in Table 1, we would expect a molecular disorientation of  $\pm 13.6^\circ$  to fulfill the observed large adsorbed density. However, we finally show that, due to specific triphenylene core–Au(111) interactions, only two diastereoisomers may exist instead of four, corresponding to  $\beta = \pm 27.4^\circ$ . The *M*0 and *M*3 chirality, deduced on the basis of twofold orientation of domains consisting of equidistant lattice nodes residing on the surface sites of similar potential, could not be directly evidenced from STM images. A theoretical analysis finally appears instrumental in elucidating the chiral character of the structures.

Two meshes over a number of 11 commensurate structures are finally selected: in the first one, *M*3, the interactions between triphenylene core and substrate are dominating, while the second one, *M*0, benefits from the stabilizing alkyl chains. We discovered the specificity for the triphenylene core/Au substrate interaction, leading to a favorable interaction for the orientation of the triangular motif of the triphenylene core with its apexes pointing in the Au<110> directions, the energetical advantage being larger than 0.26 eV per triphenylene core. For triphenylene molecules with C<sub>5</sub>H<sub>11</sub> alkyl chains, this latter geometry appears to be of similar energy to the one with three out of six chains oriented parallel to the Au<110>. Consequently, our results also suggest that for alkoxy chains shorter than pentyloxy, the core may be oriented parallel to the Au<110> for all molecules. For chains longer than C<sub>5</sub>H<sub>11</sub>, we expect in contrast disoriented triphenylene cores. This finally suggests that increasing the alkoxy chains length would also select only one kind of adsorbed mesh, the latter one. Ultimately (for increasing *n* further), we can even expect that the monolayer loses the hexagonal symmetry, which would definitely allow a larger number of alkoxy chains in epitaxy with respect to Au(111). This last event has been well described previously, with the H11T forming row-like structures on Au(111),<sup>26,33</sup> or on graphite for alkoxy chains of length longer than 12 carbons.<sup>34</sup>

## CONCLUSIONS

In this Article we present a detailed description of the self-assembly of HST, a discotic molecule, on Au(111). Although HST and its several homologues have been studied previously on different substrates, here we evidence the emergence of chirality in two structures that coexist in the monolayer. By combining both experimental and theoretical approach we evidence the commensurability of the two structures, respectively (7 × 7) and ( $\sqrt{52} \times \sqrt{52}$ )R13.9°. Our calculations show that the maximization of molecular density on the substrate leads to a rotation of the molecules with respect to the crystallographic axes of the molecular network—to avoid steric repulsion between neighboring alkoxy chains. This rotation

plays a major role in the emergence of chirality together with the induced commensurability of the adsorbed molecular structures. For large adsorbed molecules, commensurability implies large structures and therefore potential disorientations of the molecular network with respect to the high symmetry directions of the underlying substrate. Moreover, we evidence that the Au(111) substrate stabilizes only few of the potentially allowed adsorbed structures, as a result of the dual nature of interfacial interactions. ( $\sqrt{52} \times \sqrt{52}$ )R13.9° domains benefit from the triphenylene (aromatic) core interactions with gold while the (7 × 7) structure is stabilized by the three out of six pentyl chains for each molecule. We thus evidence a specifically stabilized orientation for the triphenylene core with its symmetry axes collinear to the Au<110>. This orientation represents an energy advantage at least larger than 0.26 eV with respect to the disoriented core. Moreover, we demonstrate that HST constitutes an interesting example where equilibrated contributions from both aromatic and aliphatic counterparts are present. This appears in contrast with longer peripheral substituents, i.e., H11T, for which alkyl part dominates the organization of the monolayer that is manifested by the hexagonal symmetry breaking.<sup>26,33</sup>

## AUTHOR INFORMATION

### Corresponding Authors

\*E-mail: bernard.croset@upmc.fr.

\*E-mail: emmanuelle.lacaze@upmc.fr.

### Notes

The authors declare no competing financial interest.

## ACKNOWLEDGMENTS

We thank European Community for financial support corresponding to INCO project, FP7 Marie Curie ILSES project No. 612620 and Nanotwining FP7 Project ID294952.

## REFERENCES

- (1) Katsonis, N.; Lacaze, E.; Feringa, B. L. Molecular chirality at fluid/solid interfaces: Expression of asymmetry in self-organised monolayers. *J. Mater. Chem.* **2008**, *18*, 2065–2073.
- (2) Ernst, K.-H. Supramolecular surface chirality. *Top. Curr. Chem.* **2006**, *265*, 209–252.
- (3) Xu, H.; Ghijssens, E.; George, S. J.; Wolfs, M.; Tomovic, Z.; Schenning, A. P. H. J.; De Feyter, S. Chiral induction and amplification in supramolecular systems at the liquid–solid interface. *ChemPhysChem* **2013**, *14*, 1583–1590.
- (4) Katsonis, N.; Xu, H.; Haak, R. M.; Kudernac, T.; Tomovic, Z.; George, S.; Van der Auweraer, M.; Schenning, A. P. H. J.; Meijer, E. W.; Feringa, B. L.; De Feyter, S. Emerging solvent-induced homochirality by the confinement of achiral molecules against a solid surface. *Angew. Chem., Int. Ed.* **2008**, *47*, 4997–5001.
- (5) Tahara, K.; Yamaga, H.; Ghijssens, E.; Inukai, K.; Adisoejoso, J.; Blunt, M. O.; De Feyter, S.; Tobe, Y. Control and induction of surface-confined homochiral porous molecular networks. *Nat. Chem.* **2011**, *3*, 714–719.
- (6) Masini, F.; Kalashnyk, N.; Knudsen, M. M.; Cramer, J. R.; Lægsgaard, E.; Besenbacher, F.; Gothelf, K. V.; Linderoth, T. R. Chiral induction by seeding surface assemblies of chiral switches. *J. Am. Chem. Soc.* **2011**, *133*, 13910–13913.
- (7) Parschau, M.; Romer, S.; Ernst, K.-H. Induction of homochirality in achiral enantiomorphous monolayers. *J. Am. Chem. Soc.* **2004**, *126*, 15398–15399.
- (8) De Feyter, S.; Grim, P. C. M.; Rücker, M.; Vanoppen, P.; Meiners, C.; Sieffert, M.; Valiyaveettil, S.; Müllen, K.; De Schryver, F. C. Expression of chirality by achiral coadsorbed molecules in chiral

- monolayers observed by STM. *Angew. Chem., Int. Ed.* **1998**, *37*, 1223–1226.
- (9) De Cat, I.; Guo, Z.; George, S. J.; Meijer, E. W.; Schenning, A. P. H. J.; De Feyter, S. Induction of chirality in an achiral monolayer at the liquid/solid interface by a supramolecular chiral auxiliary. *J. Am. Chem. Soc.* **2012**, *134*, 3171–3177.
- (10) Zhao, J.-S.; Ruan, Y.-B.; Zhou, R.; Jiang, Y.-B. Memory of chirality in J-type aggregates of an achiral perylene dianhydride dye created in a chiral asymmetric catalytic synthesis. *Chem. Sci.* **2011**, *2*, 937–944.
- (11) Guo, Z.; De Cat, I.; Van Averbeke, B.; Lin, J.; Wang, G.; Xu, H.; Lazzaroni, R.; Beljonnie, D.; Meijer, E.W.; Schenning, A. P. H. J.; De Feyter, S. Nucleoside-assisted self-assembly of oligo(p-phenylenevinylene)s at liquid/solid interface: Chirality and nanostructures. *J. Am. Chem. Soc.* **2011**, *133*, 17764–17771.
- (12) Samori, P.; Rabe, J. P. Scanning probe microscopy explorations on conjugated (macro) molecular architectures for molecular electronics. *J. Phys.: Condens. Matter* **2002**, *14*, 9955–9973.
- (13) De Feyter, S.; Uji-i, H.; Mamoudou, W.; Miura, A.; Zhang, J.; Jonkheijm, P.; Schenning, A. P. H. J.; Meijer, E. W.; Chen, Z.; Wurthner, F.; Schuurmans, N.; Van Esch, J.; Feringa, B. L. Supramolecular chemistry at the liquid/solid interface probed by scanning tunnelling microscopy. *Int. J. Nanotechnol.* **2006**, *3*, 462–479.
- (14) Frommer, J. Scanning tunneling microscopy and atomic force microscopy in organic chemistry. *Angew. Chem., Int. Ed.* **1992**, *31*, 1298–1328.
- (15) Weckesser, J.; De Vita, A.; Barth, J.; Cai, C.; Kern, K. Mesoscopic correlation of supramolecular chirality in one-dimensional hydrogen-bonded assemblies. *Phys. Rev. Lett.* **2001**, *87*, 096101.
- (16) De Feyter, S.; De Schryver, F. C. Two-dimensional supramolecular self-assembly probed by scanning tunneling microscopy. *Chem. Soc. Rev.* **2003**, *32*, 139–150.
- (17) Hermann, B. A.; Scherer, L. J.; Housecroft, C. E.; Constable, E. C. Self-organized monolayers: A route to conformational switching and read-out of functional supramolecular assemblies by scanning probe methods. *Adv. Funct. Mater.* **2006**, *16*, 221–235.
- (18) Humblot, V.; Ortega Lorenzo, M.; Baddeley, C. J.; Haq, S.; Raval, R. Local and global chirality at surfaces: Succinic acid versus tartaric acid on Cu(110). *J. Am. Chem. Soc.* **2004**, *126*, 6460–6469.
- (19) Charra, F.; Cousty, J. Surface-induced chirality in a self-assembled monolayer of discotic liquid crystal. *Phys. Rev. Lett.* **1998**, *80*, 1682–1685.
- (20) Richardson, N. V. Adsorption-induced chirality in highly symmetric hydrocarbon molecules: Lattice matching to substrates of lower symmetry. *New J. Phys.* **2007**, *9*, 395.
- (21) Schöck, M.; Otero, R.; Stojkovic, S.; Hümmelink, F.; Gourdon, A.; Lægsgaard, E.; Stensgaard, I.; Joachim, C.; Besenbacher, F. Chiral close-packing of achiral star-shaped molecules on solid surfaces. *J. Phys. Chem. B* **2006**, *110*, 12835–12838.
- (22) Billard, J.; Dubois, J. C.; Tinh, N. H.; Zann, A. Mesophase of disc-like molecules. *Nouv. J. Chim.* **1978**, *2*, 535–540.
- (23) Słeczkowski, P.; Katsonis, N.; Marchenko, A.; Lacaze, E. Two-fold orientation of triphenylene-based discotic liquid crystals on gold. *Mol. Cryst. Liq. Cryst.* **2012**, *558*, 102–108.
- (24) Fisher, A.; Blöchl, P. Adsorption and scanning-tunneling-microscope imaging of benzene on graphite and MoS<sub>2</sub>. *Phys. Rev. Lett.* **1993**, *70*, 3263–3266.
- (25) Markovitsi, D.; Germain, A.; Millie, P.; Lecuyer, P.; Gallos, L.; Argyrakis, P.; Bengs, H.; Ringsdorf, H. Triphenylene Columnar Liquid Crystals: Excited States and Energy Transfer. *J. Phys. Chem.* **1995**, *99*, 1005–1017.
- (26) Perronet, K.; Charra, F. Influence of molecular-substrate interaction on the self-assembly of discotic liquid crystals. *Surf. Sci.* **2004**, *551*, 213–218.
- (27) Kitagorodskii, A. I. *Organic Chemical Crystallography*; Consultants Bureau: New York, 1962.
- (28) Libuda, J.; Scoles, G. Collision-induced desorption of hydrocarbons physisorbed on Au(111). *J. Chem. Phys.* **2000**, *112*, 1522–1530.
- (29) Marchenko, O.; Cousty, J. Molecule length-induced reentrant self-organization of alkanes in monolayers adsorbed on Au(111). *Phys. Rev. Lett.* **2000**, *84*, 5363–5366.
- (30) Yamada, R.; Uosaki, K. Two-dimensional crystals of alkanes formed on Au(111) surface in neat liquid: Structural investigation by scanning tunneling microscopy. *J. Phys. Chem. B* **2000**, *104*, 6021–6027.
- (31) Uosaki, K.; Yamada, R. Formation of two-dimensional crystals of alkanes on the Au(111) surface in neat liquid. *J. Am. Chem. Soc.* **1999**, *121*, 4090–4091.
- (32) Yoon, B.; Luedtke, W.; Gao, J.; Landman, U. Diffusion of gold clusters on defective graphite surfaces. *J. Phys. Chem. B* **2003**, *107*, 5882–5891.
- (33) Katsonis, N.; Marchenko, A.; Fichou, D. Substrate-induced pairing in 2,3,6,7,10,11-hexakis-undecalkoxy-triphenylene self-assembled monolayers on Au(111). *J. Am. Chem. Soc.* **2003**, *125*, 13682–13683.
- (34) Wu, P.; Zeng, Q.; Xu, S.; Wang, C.; Yin, S.; Bai, C.-L. Molecular superlattices induced by alkyl substitutions in self-assembled triphenylene monolayers. *ChemPhysChem* **2001**, *2*, 750–754.